# Adopting the Principles of Collagen Biomineralization for Intrafibrillar Infiltration of Yttria-Stabilized Zirconia into Three-Dimensional Collagen Scaffolds

*Bin Zhou, Li-na Niu,* Wei Shi, Wei Zhang, Dwayne D. Arola, Lorenzo Breschi, Jing Mao, Ji-hua Chen,* David H. Pashley, and Franklin R. Tay**

**In this paper, a process for generating collagen-yttria-stabilized amorphous zirconia hybrid scaffolds by introducing acetylacetone-inhibited zirconia precursor nanodroplets into a poly(allylamine)-coated collagen matrix is reported. This polyelectrolyte coating triggers intrafibrillar condensation of the precursors into amorphous zirconia, which is subsequently transformed into yttria-stabilized zirconia after calcination. These findings represent a new paradigm in the synthesis of non-naturally occurring collagen-based hybrid scaffolds under alcoholic mineralizing conditions.**

## 1. Introduction

Zirconia-based ceramics are well known for their unusual combination of mechanical strength, ionic conductivity, thermal stability and optical properties.[1] These ceramics, particularly in the form of yttria-stabilized zirconia (YSZ), have important commercial applications such as oxygen sensors and as solid electrolytes in solid oxide fuel cells due to their high oxygen-ionic conductivity while blocking electronic conduction.[2–4] Sol–gel strategies based on hydrolysis of metal alkoxides and followed by a condensation reaction have been used to produce zirconia powders[5] and thin films [6] with high degrees of purity. Many organofunctional zirconia molecules have been used to produce sol-gel derived zirconia with well-defined micro- and macro-structures.[7–9] Recently, a method for incorporating zirconium dioxide nanophase in chitinous scaffolds has been reported.[10] Nevertheless, the method requires synthesis under high temperature (150 °C) and may not be applicable for other biological scaffolds that denature at this processing temperature.

Because of its hierarchical tertiary structure and biocompatibility, type I collagen has been used as bio-templates for creating organic-inorganic hybrid materials at ambient temperature with three-dimensional structural hierarchy. To date, most of the studies are targeted at biomimetic replication of the natural process of biomineralization.[11] These biomimetic processes are generally achieved via the creation of amorphous calcium carbonate or calcium phosphate precursors in an initial dense liquid state;[12] the liquid-like characteristics of these precursor phases enable them to diffuse into the intrafibrillar water compartments of fibrillar collagen. Following infiltration into the collagen fibrillar template, the mineral precursors further densify by losing bound water and undergo phase transformation into nanocrystalline calcite/aragonite or octacalcium phosphate/apatite within the intrafibrillar milieu of collagen fibrils.[13,14]

Unlike amorphous calcium carbonate or calcium phosphate that can be transformed into crystalline mineral phases at ambient temperature, minerals such as amorphous silica or zirconia require sintering to high temperatures before crystalline transformation occurs. For zirconia, pure tetragonal and cubic crystalline phases are metastable at ambient temperature and require dopants such as yttria,[15] ceria,[16] or other rare earth element oxides to inhibit hydrothermal tetragonal-to-monoclinic phase transition and stabilize the sintered crystalline zirconia at ambient temperature. Here, we report a process for generating collagen-yttria-stabilized amorphous zirconia hybrid three-dimensional scaffolds by introducing acetylacetone-inhibited zirconia precursor nanodroplets into a poly(allylamine)-coated collagen matrix. This polyelectrolyte coating triggers intrafibrillar condensation of the precursors into amorphous zirconia, which may subsequently be transformed into tetragonal YSZ after calcination. The hypothesis tested in the present work is that the principle of collagen biogenic mineralization may be

Dr. B. Zhou, Dr. W. Shi, Dr. W. Zhang, Prof. J. Mao
Tongji Hospital
Huazhong University of Science and Technology
Wuhan, P. R. China
Dr. L.-N. Niu, Prof. J.-H. Chen
Department of Prosthodontics
School of Stomatology
Fourth Military Medical University
Xi'an, P. R. China
E-mail: niulina831013@126.com; jhchen@fmmu.edu.cn
Prof. D. D. Arola
Department of Mechanical
University of Maryland Baltimore County
Baltimore, MD, USA
Prof. L. Breschi
Department of Biomedical and Neuromotor Sciences
DIBINEM, University of Bologna and IGM-CNR
Bologna, Italy
Prof. D. H. Pashley, Prof. F. R. Tay
Georgia Regents University
Augusta, GA, 30912–1129, USA
E-mail: ftay@gru.edu

**DOI: 10.1002/adfm.201302920**

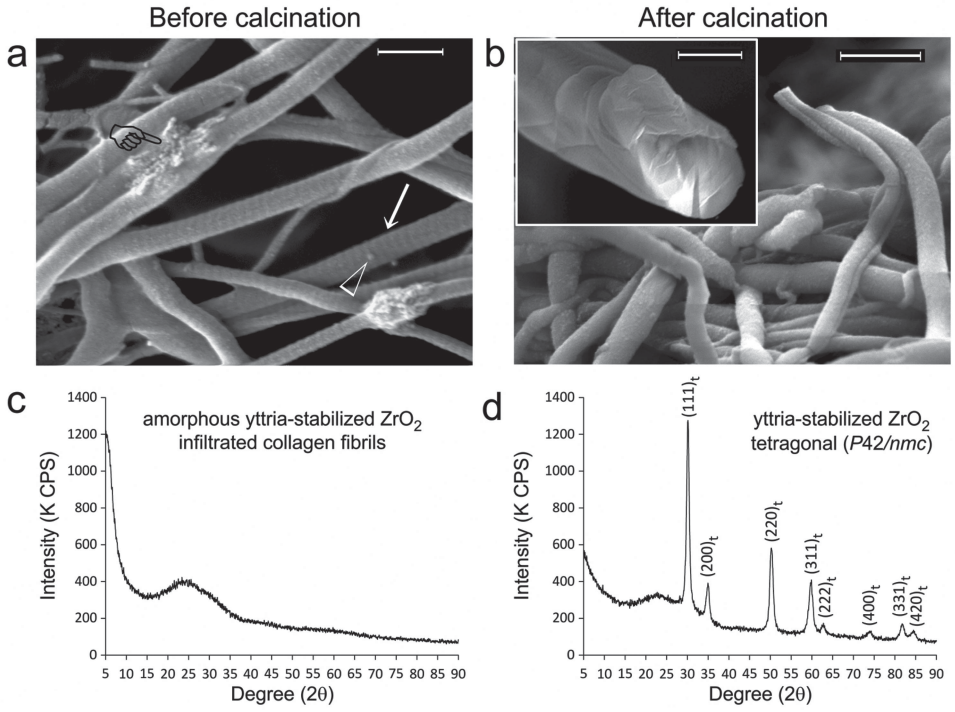


**Figure 1.** Infiltration of yttrium-stabilized zirconia (YSZ) into reconstituted type I collagen scaffolds. Scanning electron microscopy images of YSZ-infiltrated collagen fibrils a) before (bar = 500 nm) and b) after calcination (bar = 500 nm). Prior to calcination, fibrils infiltrated with YSZ appear cylindrical, do not collapse when examined under high vacuum and demonstrate surface cross-banding patterns (arrow). Intrafibrillar YSZ can be vaguely discerned within fibrils that are partially squashed during handling (pointer). Open arrowhead: spherical particles probably represent extrafibrillar amorphous YSZ aggregates that have not been completely removed after rinsing the mineralized scaffolds with 1-propanol. After calcination to 800 °C, cross-banding patterns disappeared in the organic matter-depleted mineralized fibrils. Inset: fractured section of a calcined fibril with a uniformly dense solid mineral core provides the evidence for successful intrafibrillar YSZ infiltration prior to calcination (bar = 200 nm). Powder X-ray diffraction of YSZ-infiltrated collagen sponges c) before and d) after calcination. Before calcination, the infiltrated mineral is probably amorphous YSZ. After calcination, the amorphous zirconia phase is partially converted into a crystalline phase, with *hkl* crystal lattice peak designations corresponding to tetragonal zirconia (JCPDF number 42–1164).

adopted for biomimetic infiltration of non-naturally occurring minerals in the intrafibrillar milieu of a three-dimensional reconstituted or naturally-occurring collagen matrix.

## 2. Results and Discussion

A YSZ precursor solution in propanol was prepared using acetylacetone (acac),1-propanol, zirconium (IV) propoxide [$Zr(OPr)_4$], yttrium (III) nitrate hexahydrate, and water in the molar ratio 1.2:45.4:2:0.2:20 (Supporting Information, S1). The solution's pH was adjusted from 3.85 to 5.0 with $NH_4OH$ to control the rate of hydrolysis. As $Zr(OPr)_4$ is very sensitive to moisture, acac was used as an inhibitor, in the form of a bidentate complexing ligand $[Zr(OPr)_3(acac)]_2$,[17] to decrease the rate of condensation.[18] The yellow (charge-transfer coloration) acac-inhibited YSZ precursor sol was stable, without gelation, for more than 90 days when stored at ambient temperature.[19]

We employed glutaraldehyde for grafting of poly(allylamine) hydrochloride (PAH) to a three-dimensional collagen matrix, in order to create a polyelectrolyte capsule around the collagen molecules to enhance the infiltration of YSZ precursors. This procedure is critical for successful intrafibrillar infiltration of the YSC precursors into the collagen fibrils, as control experiments indicated that those precursors only deposited along the surface of the collagen fibrils in the absence of PAH grafting (Supporting Information, S2).Grafting of reconstituted type I collagen scaffolds with PAH was achieved by incubating the scaffolds with $6.67 \times 10^{-4}$ M PAH for 4 hours and then in 1.5 wt% glutaraldehyde for 4 h to cross-link the PAH to collagen. The PAH-grafted scaffolds were subsequently immersed in acac-inhibited YSZ precursor solution for 12 days. Macroscopically, air-dried zirconified collagen scaffolds are capable of maintaining their rehydrated, expanded status without collapsing (Supporting Information, S3). Scanning electron microscopy of YSZ-infiltrated scaffolds (**Figure 1**a) reveal cylindrical collagen fibrils with cross-banded appearance after intrafibrillar infiltration with amorphous YSZ. Calcination of YSZ-infiltrated collagen scaffolds to 800 °C results in solid cores of mineralized fibrils (Figure 1b). Powder X-ray diffraction of YSZ-infiltrated collagen scaffolds before calcination yields an amorphous diffraction pattern (Figure 1c). After calcination, the amorphous zirconia is partially-converted into a crystalline phase with *hkl* lattice designations corresponding to tetragonal zirconia ($P4_2/nmc$; Figure 1d).[20] We used 10 mol% $YO_{1.5}$ to stabilize the calcined zirconia (i.e., aliovalent alloying) to prevent martensitic transformation of the metastable tetragonal phase of pure zirconia into monoclinic zirconia at low

temperature.[21,22] A higher concentration of doped yttrium (>4.5 mol% $Y_2O_3$) also lowers the transition temperature for tetragonal-cubic phase transformation.[1,23]

To understand the kinetics of YSZ precursor infiltration into PAH-grafted collagen scaffolds, we performed transmission electron microscopy (TEM) of those scaffolds that had been immersed in acac-inhibited YSZ precursors for 24 h, 8 and 12 days. Initially, the YSZ precursors existed as loose, uncoalesced nano-clusters (<2 nm in diameter; Supporting Information, S4), which in the vicinity of a functionalized collagen substrate, coalesced into larger amorphous aggregates (**Figure 2**a). These nano-clusters probably corresponded to the TEM appearance

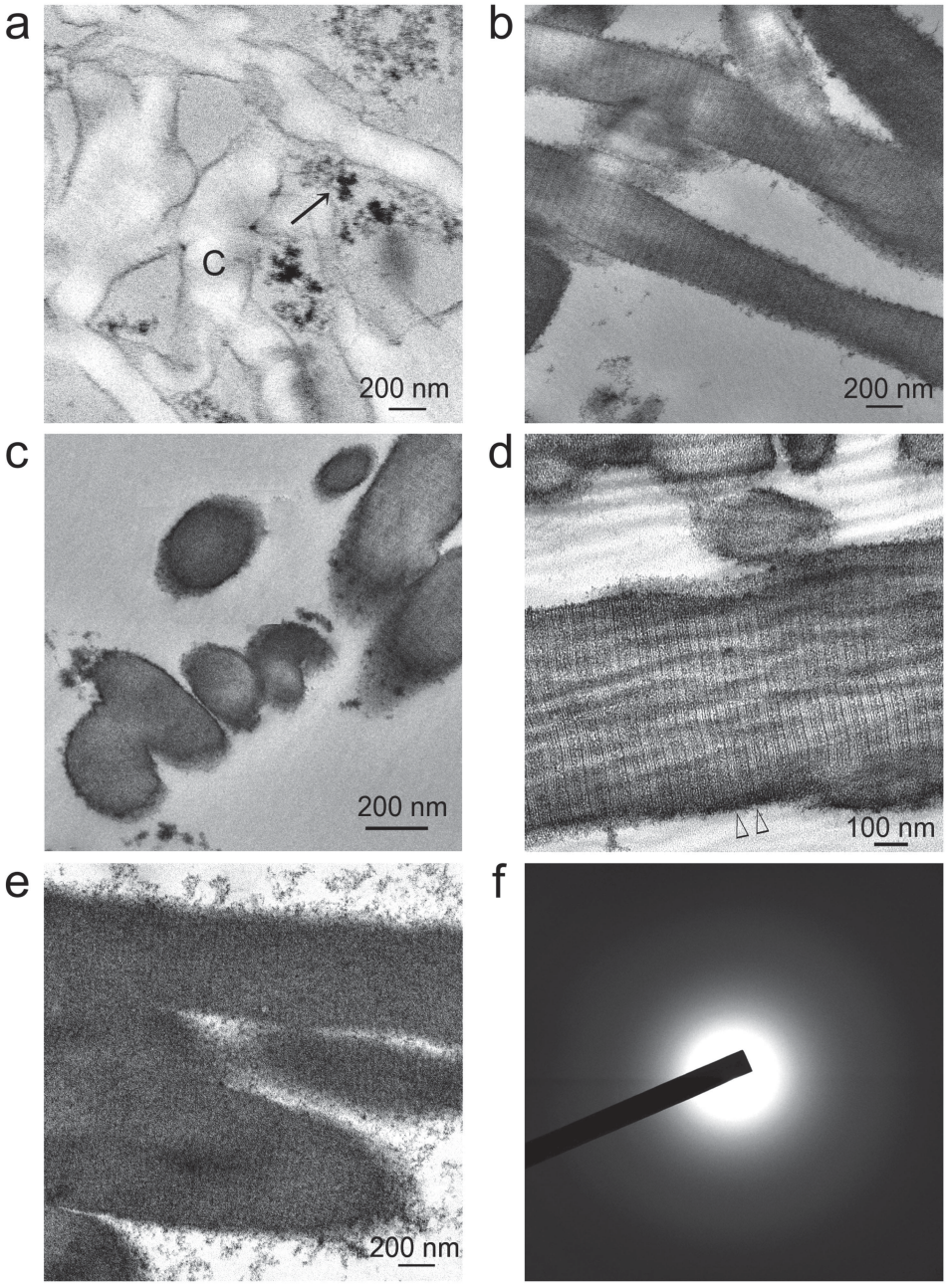


**Figure 2.** Transmission electron microscopy of non-osmicated, unstained sections showing the time-course of events after poly(allylamine) and glutaraldehyde pre-treated collagen scaffolds were immersed in a solution containing acac-inhibited YSZ precursors. a) After 24 h, electron-dense extrafibrillar YSZ precursors (arrow) can be seen around the non-infiltrated collagen fibrils (C). b) After 4 days, discontinuous electron-dense, amorphous (selected area electron diffraction not shown) intrafibrillar minerals can be discerned within some collagen fibrils. Cross-banding can be vaguely discerned in those infiltrated regions (pointers). c) Cross section of ziconified collagen fibrils showing mineral infiltration from the surface to the center of the fibrils. d) After 8 days, intrafibrillar infiltration of amorphous YSZ is intense enough for distinctive cross-banding patterns with 67 nm wide D-spacing (between open arrowheads) and rope-like microfibrillar architecture to be visible across the entire length of the collagen fibrils. e) After 12 days, collagen cross banding and microfibrillar architecture are obscured by the densely infiltrated, intrafibrillar amorphous YSZ. f) Selected area electron diffraction reveals the amorphous nature of the infiltrated minerals in (e).

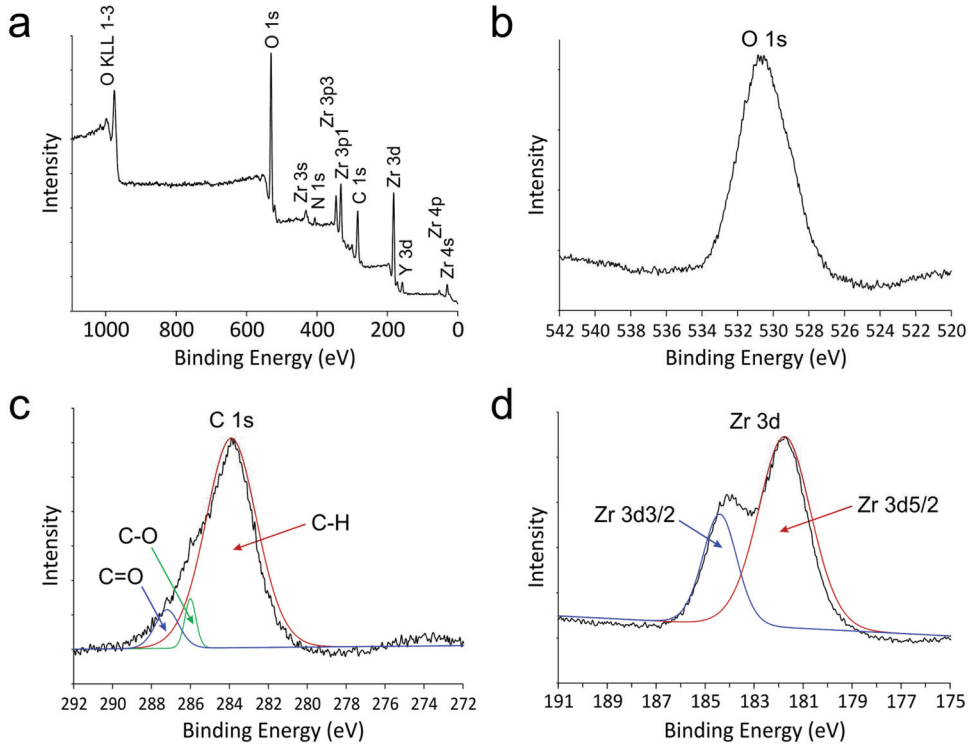


**Figure 3.** X-ray photoelectron spectroscopy (XPS) characterization of YSZ-infiltrated collagen scaffold. a) Survey spectrum of the as-prepared, non-calcined sponges. b) High resolution spectrum of O 1s reveals only one peak at 530.8 eV that is derived from $ZrO_2$. Absence of OH is indicative of complete conversion of $Zr(OH)_4$ into amorphous zirconia. c) High resolution deconvoluted spectrum of C 1s reveals 3 peaks at 283.9, 286.0, and 287.2 eV that may be assigned to the C–H, C–O, and C=O bonds, respectively. These three peaks are derived from the organic components of the collagen matrix. d) High resolution deconvoluted spectrum of Zr 3d reveals two peaks at 181.8 and 184.4 eV that may be assigned to Zr 3d5/2 and Zr 3d3/2, respectively. The detected binding energies are higher than those reported for Zr metal (180.0 eV) and ZrO*x* ($0 < x < 2$, 181.4 eV).

of prenucleation clusters that were recently identified in calcium carbonate[24] and calcium phosphate systems[25,26] and during magnetite synthesis.[27] Up to 4 days, amorphous aggregates of YSZ precursors were found to infiltrate the interior of unstained collagen fibrils, wherein there was fluctuation in the density of the aggregates which corresponding to the banding patterns of the collagen fibrils (Supporting Information, S4). At 8 days, intrafibrillar infiltration of amorphous YSZ resulted in the appearance of 67 nm wide cross-banding patterns and rope-like microfibrillar architecture within the unstained collagen fibrils (Figures 2d). At 12 days, these ultrastructural characteristics were obscured by as the intrafibrillar YSZ densified, producing fibrils containing densely-infiltrated amorphous YSZ (Figure 2e,f).

Infrared spectrum collected from YSZ-infiltrated collagen scaffolds demonstrates amide peaks derived from type I collagen and Zr–O peaks derived from acac-inhibited YSZ precursors (Supporting Information, S5a). Identification of C–O bands derived from acac [28] as a chelating ligand for $Zr(OH)_4$ suggests that remnants of the precursors are present in the zirconified collagen scaffold. This corresponds with TEM observation of YSZ precursor aggregates along the surface of mineralized collagen fibrils (Figure 2e). Energy-dispersive X-ray analysis (EDX) of YSZ-infiltrated scaffolds indicates the presence of doped yttrium within the bulk of the zirconified organic matrix (Supporting Information, S5b).

The chemical state of amorphous YSZ along the surface of cryofractured mineralized collagen scaffolds was investigated using X-ray photoelectron spectroscopy (XPS), with which properties of the inner-shell electrons were probed. A wide-scan survey spectrum (**Figure 3**a) identified the elemental composition previously determined by EDX. High resolution narrow-scan spectra and peak deconvolutions were performed for the O1s, C1s, and Zr3d core levels. The O1s spectrum (Figure 3b) reveals only one peak at 530.8 eV; absence of a deconvoluted OH peak may be due to complete condensation of $Zr(OH)_4 \cdot n$H2O into hydrous amorphous zirconia ($ZrO_2 \cdot nH_2O$) within the freeze-fractured mineralized fibrils.[29] The three deconvoluted peaks at 284.9, 286.7, and 288.0 eV in the C1s spectrum (Figure 3c) are ascribed to C–H, C–O, and C=O bonds, respectively,[30] which are predominantly attributed to the organic components derived from collagen. The two deconvoluted peaks at 181.8 and 184.4 eV in the Zr3d spectrum (Figure 3d) are ascribed to spin-orbit splitting of the Zr3d components, Zr3d5/2 and Zr3d3/2, respectively. The binding energy for Zr3d5/2 is higher than that reported for Zr metal (180.0 eV) but lower than zirconia (182.2 eV).[31] The lower binding energy between the Zr nucleus and inner electrons, as compared to pure $ZrO_2$, probably arises from the presence of chemical bonding between the inorganic core and organic components, which may be attributed to incomplete hydrolysis of the zirconium alkoxide precursors.

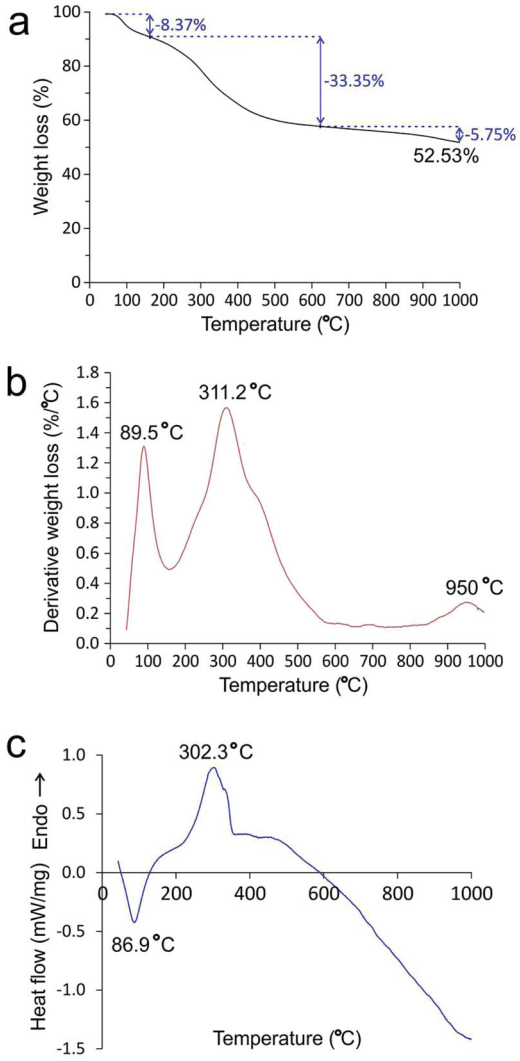


**Figure 4.** Thermal analyses of YSZ-infiltrated collagen scaffolds. a) Thermogravimetric analysis. b) Derivative weight loss. The total weight loss from a representative YSZ-infiltrated collagen scaffold is 47.47%. Weight loss under 150 °C (8.37%; derivative weight loss peak at 89.5 °C) is attributed to the loss of physisorbed water. Weight loss from 150–630 °C (derivative weight loss peak at 302.3 °C) is associated with loss of chemically-bound water, decomposition of organic matters, which may include collagen, poly(allylamine) and glutaraldehyde-associated crosslinks. Above 630 °C, sample weight only slightly decreases, indicating organic moieties have decomposed predominantly and the crystalline $ZrO_2$ becomes very stable. The slight weight loss from 630–1000 °C (5.75%; derivative weight loss peak at 950 °C) may be attributed to the loss of lattice water during transformation of YSZ from the monoclinic to the tetragonal phase. c) Differential scanning calorimetry. The endothermic peak at 86.9 °C may be attributed to the heat required for dissipation of physisorbed water. The exothermic peak at 302.3 °C may be attributed to the heat released during oxidation and elimination of organic compounds. The small exothermic peak at 330 °C may be related to the decomposition of acac used for chelating the $Zr(OPr)_4$ precursors. Above 500 °C, the heat flow starts to decrease (endothermic), corresponding to the formation of the crystalline zirconia phase.

Thermal analyses of YSZ-infiltrated collagen scaffolds were performed using thermogravimetric analysis (TGA) and differential scanning calorimetry (DSC). The TGA data indicates that more than 50 wt% of amorphous zirconia is present within the zirconified scaffold (**Figure 4**a). Differential weight loss from the TGA yields 3 peaks at 89.5 °C, 311.2 °C, and 950 °C (Figure 4b). Weight loss under 150 °C (8.37%) is attributed to the loss of physisorbed water. Weight loss from 150–630 °C (33.35%) is associated with decomposition of organic matters, which may include collagen, poly(allylamine) and glutaraldehyde-associated cross-links. The second derivative weight loss peak at 311.2 °C is higher than that recorded for glutaraldehyde cross-linked mineral-free collagen scaffolds (299.4 °C; data not shown). Thus, binding of amorphous zirconia to PAH-grafted collagen improves the thermal stability of collagen fibrils, and may increase their degradation resistance against bacterial collagenase and tissue matrix metalloproteinases, a desirable property exhibited by the presence of intrafibrillar apatite crystallites in mineralized hard tissues.[32] Above 630 °C, sample weight slightly decreases, indicating organic moieties have decomposed predominantly and the crystalline $ZrO_2$ becomes very stable. The slight weight loss from 630–1000 °C (5.75%; derivative weight loss peak at 950 °C) may be attributed to the loss of lattice water incorporated in tetragonal zirconia.[1,33] From the DSC data (Figure 4c), the endothermic peak at 86.9 °C is attributed to the heat required for evaporation of physisorbed water. The exothermic peak at 302.3 °C is attributed to the heat released during oxidation of organic compounds. Above 500 °C, the heat flow starts to decrease (endothermic), corresponding to the formation of the crystalline zirconia phase.

To verify that intrafibrillar zirconification strategy can be reproduced in natural collagen scaffolds, we repeated our experiments with PAH-grafted soft tissue collagen derived from rat-tail tendon and demineralized, delipdated porcine trabecular bone. The parallel fibrillar arrangement in the rat-tail tendon enables electron-dense amorphous YSZ mineral phase within the PAH-grafted collagen fibrils to be more clearly identified by TEM (Supporting Information, S6). Similar cross-banding characteristics were observed as in the reconstituted collagen scaffolds. As TEM techniques only show the extent of YAZ infiltration on one plane of the sectioned scaffold at the nanometer length scale, we resorted to the use of micro-computed tomography of porcine cancellous bone specimens remineralized with amorphous YSZ to examine the uniformity of YSZ infiltration at the millimeter scale. Homogeneous zirconification of the surface and interior environment of the demineralized collagen matrix can be seen from a piece of trabecular bone (**Figure 5**). A movie prepared from the 3-D reconstructed images is registered under the name "YSZ infiltrated demineralized trabecular bone.avi",[34] which provides a three-dimensional view of the external surface and the interior environment of the intrafibrillarly-mineralized trabecular bovine bone. Although reconstituted collagen scaffolds and cancellous bone are both highly porous in nature, they differ in the thickness of the collagen layers, with the former consisting of leaflets of collagen fibrils that are up to 50 fibrils thick. By contrast, bone trabaculae in cancellous bone contain collagen layers that are up to several hundreds of layers thick. The results indicate that the ziconification with YSZ liquid-like precursor phases is capable of remineralizing dense collagen scaffolds as long as porosities exist in the sinusoids of the cancellous bone to permit wetting of the demineralized bone trabeculae.

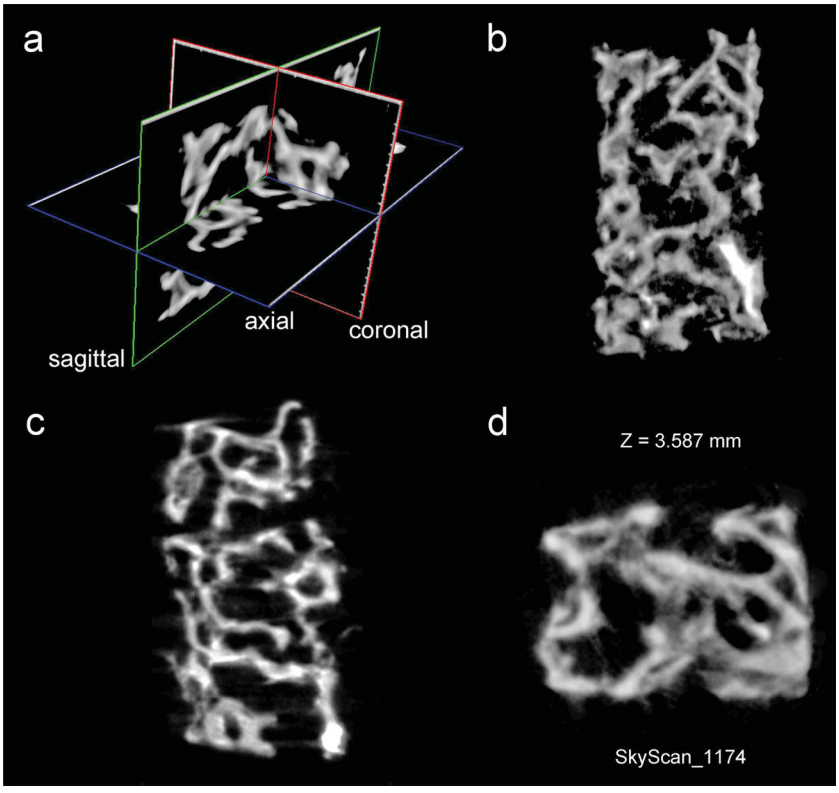


**Figure 5.** Micro-computed tomography of a piece of delipidated and demineralizedporcine trabecular bone that has been infiltrated with acac-inhibited YSZ precursors. Images represent segmentations of a reconstructed image. a) Three-dimensional visualization of the block of trabecular bone remineralized with amorphous YSZ. b) Coronal image. c) Sagittal image. d) Transaxial image.

To clarify the interaction between PAH and acac-inhibited YSZ precursors, PAH was added to the acac-inhibited YSZ precursor solution. These solutions were examined using dynamic light scattering and zeta potential measurement. The acac-inhibited YSZ precursors dispersed in 1-propanol exist as nanodroplets with a hydrodynamic diameter of 4.701 nm with a polydispersity index of 0.212, as determined by dynamic light scattering (Supporting, Information, S7-I). The dimension of the YSZ nanoparticles as determined by dynamic light scattering was larger than what was observed using TEM (Supporting Information, S4), probably due to the experimental conditions employed for dynamic light scattering; the latter may be also measuring the hydration layers of bound water surrounding the nanoparticles,[35] which cannot be readily identified using conventional TEM. When PAH was added dropwise to acac-inhibited YSZ precursor solution, condensation of the YSZ occurred and the mixture became turbid immediately. The hydrodynamic diameter of the particles in the solution increases to 659.1 nm, with a polydispersity index of 0.617 (Supporting Information, S7-I). Being two orders of magnitude larger than the acac-inhibited YSZ precursors examined without the addition of PAH, under the same dynamic light scattering experimental conditions, the results suggest a potential mechanism of the PAH grafted to the collagen in enhancing the aggregation of the initially small clusters into larger dense liquid phases and amorphous aggregates.[16] The zeta potential of acac-inhibited YSZ precursor solution also changes from 21.78 ± 0.49 mV to 28.15 ± 1.56 mV ($N$ = 2) after addition of PAH (Supporting Information, S7-II). Poly(allylamine) exists as its protonated form (pKa 8.7)[36] when added to the acac-inhibited YSZ precursor solution (pH 5.0). When these results are interpreted together with attenuated total reflection-Fourier transform infrared spectroscopy (ATR-FTIR) of the respective solution (Supporting Information, S7-III), PAH appears to recruit clusters of acac-inhibited YSZ nanoparticles into the collagen fibril and produce larger dense liquid amorphous phases with higher positive surface charges. This is probably achieved by consuming free acac and sequestering $OH^-$ ions. Once inside the collagen fibrils, water from the hydrated collagen's water-rich intrafibrillar compartments[37] induces condensation of amorphous zirconia from their acac-inhibited precursors. However, how large those amorphous mineral phases can aggregate will be restrained by the dimensions of the water compartments with the lateral intermolecular spaces between collagen molecules, the gap zones between adjacent collagen fibrils and spaces between the microfibrils.[38] Also, without further calcination, the densified aggregates will remain in their amorphous states and will not automatically transform into more highly ordered crystalline forms.

In parallel experiments in which glutaraldehyde or water is added to the acac-inhibited YSZ precursors in the absence of PAH (Supporting Information, S7-II), the precursor solution remains clear and the FTIR peaks assigned to free acac remain stable (Supporting Information, S7-III). These parallel experiments exclude the effect of glutaraldehyde (used for crosslinking PAH to collagen) or water on premature condensation of YSZ in the absence of PAH. Solid-state zeta potential measurements of untreated collagen scaffolds used in the present study indicate that they have a zeta potential of –2.65 ± 0.21 mV. Treatment of the collagen scaffolds with PAH only results in slight decrease in their negative zeta potential to –0.91 ± 0.28 mV, whereas further crosslinking of the PAH-treated collagen scaffolds with glutaraldehyde results in a positive zeta potential of 0.70 ± 0.09 mV ($N$ = 2) (Supporting Information, S7-IV). The PAH with its protonated positive $NH^{3+}$ domain is initially adsorbed to the collagen molecules via electrostatic interaction. Further treatment with glutaraldehyde enables the PAH molecules to be chemically fixed to the surface of the collagen molecules. Glutaraldehyde has been used to fabricate polyelectrolyte multilayers capsule over collagen by crosslinking the amine moieties derived from PAH and collagen.[39] A similar process is probably involved in the present study, with the formation of a polyelectrolyte capsule of PAH around the collagen molecules.

To validate the mechanism of formation of YSZ inside collagen matrices, we sintered YSZ-infiltrated reconstituted

collagen scaffolds to 1600 °C to convert the infiltrated mineral from amorphous to crystalline zirconia. Embedded specimens were subjected to ultramicrotomy and ultrathin sections were observed using TEM. The presence of solid leaflets of zirconia is in support of the presence of homogeneous intrafibrillar infiltration of YSZ into the collagen scaffolds (**Figure 6**a). High magnification of the zirconia indicates that the sintered material exists in the form of nanoparticles that are approximately 5 nm in diameter (Figure 6b). Even with removal of bound water from the amorphous phases after sintering and accompanied contraction, the diameter of these crystalline phases is larger than the original amorphous YSZ nano-clusters that exist prior to infiltration into the collagen matrix (Supporting information, S4-a). Selected area electron diffraction of the crystalline mineral phase revealed ring patterns that are characteristic of the tetragonal structure of the sintered polycrystalline YSZ nanoparticles (Figure 6c).

**Figure 7** schematically illustrates the hypothesized events of the infiltration and condensation of YSZ precursor nano-clusters in a PAH pre-treated, glutaraldehyde crosslinked collagen scaffold via the hydrolysis and condensation of acac-inhibited YSZ precursors. The YSZ precursor solution provides the mineral phase of nano-size particles (small green spheres) that can infuse the water compartments of a collagen fibril. Formation of a polyelectrolyte single layer (blue network) over the triple-helix of collagen molecules (red) initiates coalescence of the YSZ precursor nano-clusters into larger amorphous liquid aggregates (large green spheres), which, because of their liquid-like characteristics, continue to infiltrate the intrafibrillar milieu of the collagen fibril. Water from the intrafibrillar compartments of the collagen fibril further triggers condensation of the liquid precursor droplets into YSZ nanoparticles (black rectangles).

## 3. Conclusions

We have shown that yttria-stabilized zirconia may be introduced hierarchically into a collagen scaffold under water-sparse conditions via a propanol-based mineralizing medium. The results of the present work provide the proof-of-concept that the protocol employed allows guided intrafibrillar deposition of YSZ nanoparticles within a collagen template. While the fusion of the intrafibrillarly-deposited YSZ particles into fused YSZ with superior mechanical properties requires a sintering temperature (>2300 °C) and environmental sintering conditions that are beyond the capability of our laboratory, the strategy developed provides a means for using natural collagen templates such as demineralized fish scales or bone segments to produce fused YSZ with high mechanical strength that would have potential applications as armor components or replacement parts for damaged hard tissues of the human body.

## 4. Experimental Section

*Preparation of Acetylacetone–Inhibited, Yttria-Stabilized Zirconia (YSZ) Precursor*: A YSZ precursor solution was prepared by mixing 0.036 mol of acetylacetone (acac; 2,4-pentanodione) with 0.5 mol of 1-propanol, and

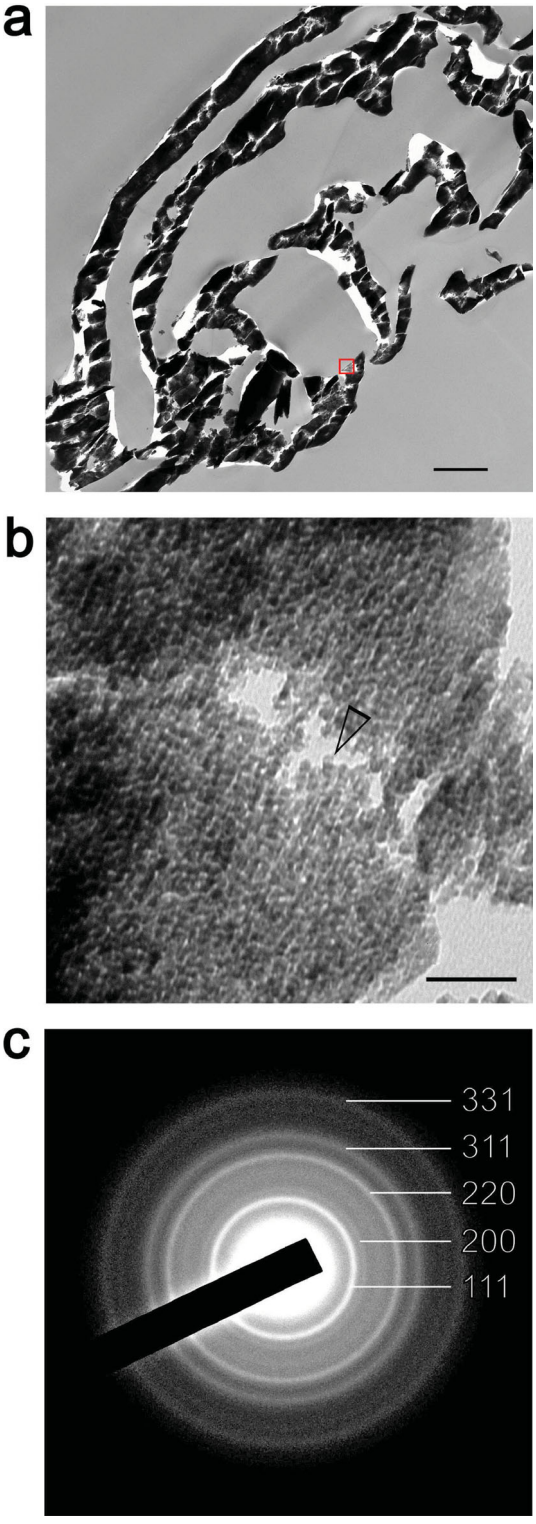


**Figure 6.** YSZ-infiltrated collagen scaffold that has been sintered in atmospheric air to 1000 °C. a) low magnification image of a part of the organic matter-free, highly electron-dense YSZ scaffold. Bar = 1 µm. b) High magnification image taken from a leaflet of the sintered mineralized scaffold (rectangle box in (a)) showing the presence of YSZ nanoparticles (≈ 5 nm in diameter – open arrowhead). Bar = 50 nm. c) Selected area electron diffraction showing ring patterns characteristic of the tetragonal structure of the sintered polycrystalline YSZ nanoparticles.

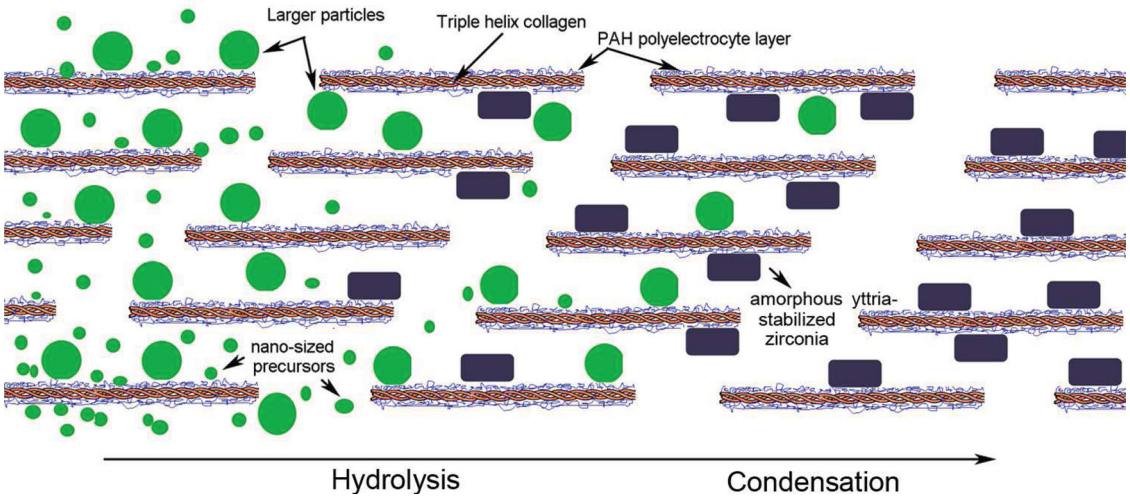


**Figure 7.** Schematic of the process of intrafibrillar deposition of yttria-stabilized zirconia (YSZ) within a collagen fibril. Acac-stablized YSZ nano-sized precursors infuse into the fibril and coalesce in the presence of the PAH-crosslinked collagen molecules to form larger-sized amorphous precusor aggregates. These aggregates further condense in the presence of water available within the intrafibrillar compartments of the collagen fibril into amorphous YSZ nanoparticles.

then adding 0.06 mol of zirconium (IV) propoxide [Zr(OPr)4] (70 wt% solution in 1-propanol) to the solution (all chemicals from Sigma-Aldrich, St. Louis, MO, USA). As $Zr(OPr)_4$ is very sensitive to moisture, acac was used as an inhibitor or a bidentate complexing ligand to decrease the condensation rate and prevent premature precipitation of $Zr(OH)_4$. The yttria precursor was obtained by dissolving 0.006 mole of yttrium (III) nitrate hexahydrate (Sigma-Aldrich) in 0.5 mol of 1-propanol. The yttria precursor solution was added to the acac-inhibited $Zr(OPr)_4$ solution under stirring. For hydrolysis of the YSZ precursor, a mixture of 0.6 mol water in 0.22 mol of 1-propanol was first prepared to avoid localized concentrations of water in the $Zr(OPr)_4$ solution that could induce heterogeneous gelation. The water/propanol mixture was added dropwise to the YSZ precursor solution under stirring. The final molar ratio of acac to 1-propanol, $Zr(OPr)_4$, yttrium (III) nitrate hexahydrate and water in the is 1.2: 45.4: 2: 0.2: 20. The solution pH was adjusted from 3.85 to 5.0 with 10% ammonia solution to control the rate of hydrolysis. The acac-inhibited YSZ precursor sol was found to be stable, without gelation, for at least 1 month when stored at ambient temperature.

*Collagen Mineralized in Acac-Inhibited YSZ Precursor*: Dried collagen scaffolds (2 cm × 2 cm × 0.2 cm) were obtained from reconstituted type I collagen tapes (Ace Surgical Supply Co., Inc, MA, USA). The scaffolds were rinsed and re-expanded with Milli-Q water and incubated with $6.67 \times 10^{-4}$ M of poly(allylamine) hydrochloride (PAH) for 4 h. The PAH pre-treated scaffolds were then incubated in 1.5% glutaraldehyde for 4 h to cross-link the PAH to collagen. After removal of excess glutaraldehyde with Milli-Q water, the collagen scaffolds were mineralized in 1 mL of acac-inhibited, YSZ precursor at 37 °C, with daily change of the mineralization medium. After 4, 8, and 12 days of mineralization, the YSZ-infiltrated scaffolds were rinsed with 1-propanol to remove the excess precursor solution and used for further characterizations. Rehydrated collagen scaffolds that were only cross-linked with 1.5% glutaraldehyde (i.e., without PAH pre-treatment) were immersed in the same mineralization medium for the same time periods and used as the control.

*Analytical Methods*: The analytical methods used in this work include scanning electron microscopy, transmission electron microscopy, powder X-ray diffraction, attenuated total reflection–Fourier transform infrared spectroscopy, energy dispersive X-ray analysis, X-ray photoelectron spectroscopy, thermogravimetric analysis, particle size distribution, and zeta potential analyses. Full experimental details are given in the Supporting Information, S1.

## Supporting Information

Supporting Information is available from the Wiley Online Library or from the author.

## Acknowledgments

B.Z. and L.-n.N. contributed equally to this work. This work was supported by grant R01 DE015306–06 from NIDCR (PI. David H Pashley), grant 81130078 from National Nature Science Foundation of China, grant 2012CB526704 from National Key Basic Research Program of China (PI. Jihua Chen) and the ERA award and IRRM award from Georgia Regents University (PI. Franklin R. Tay). The authors thank Michelle Burnside for secretarial support.

Received: August 20, 2013
Revised: September 8, 2013
Published online: November 18, 2013

[1] J. Chevalier, L. Gremillard, A. V. Virkar, D. R. Clarke, *J. Am. Ceram. Soc.* **2009**, *92*, 1901.
[2] J. Will, A. Mitterforfer, C. Kleinlogel, D. Perednis, L. J. Gauckler, *Solid State Ionics* **2000**, *131*, 79.
[3] F. Mauvey, P. Lenormand, C. Lalanne, F. Ansart, J. M. Bassat, J. C. Grenier, *J. Power Sources* **2007**, *171*, 783.
[4] E. O. Oh, C. M. Whang, Y. R. Lee, S. Y. Park, D. H. Prasad, K. J. Yoon, J. W. Son, J. H. Lee, H. W. Lee, *Adv. Mater.* **2012**, *25*, 3373.
[5] T. L. Wen, V. Hebert, S. Vilminot, J. C. Bernier, *J. Mater. Sci.* **1991**, *26*, 3787.
[6] A. Žalga, B. Abakevičienė, A. Žarkov, A. Beganskienė, A. Kareiva, S. Tamulevičius, *Mater. Sci.* **2011**, *17*, 191.
[7] M. Agarwal, M. R. De Guire, A. H. Heuer, *J. Am. Ceram. Soc.* **1997**, *80*, 2967.
[8] A.-M. Azad, *Mater. Lett.* **2006**, *241*, 60.
[9] Y. Cao, Y. M. Zhou, Y. Shan, H. X. Ju, X.J. Xue, *Adv. Mater.* **2006**, *18*, 1838.

[10] H. Ehrlich, P. Simon, M. Motylenko, M. Wysokowski, V. V. Bazhenov, R. Galli, A. L. Stelling, D. Stawski, M. Ilan, H. Stöcker, B. Abendroth, R. Born, T. Jesionowski, K. J. Kurzydlowski, D. C. Meyer, *J. Mater. Chem. B* **2013**, *1*, 5092.
[11] L. Wang, T. Azaïs, M. Robin, A. Vallée, C. Catania, P. Legriel, G. Pehau-Arnaudet, F. Babonneau, M-M. Giraud-Guille, N. Nassif, *Nat. Mater.* **2012**, *11*, 724.
[12] J. R. Dorvee, A. Veis, *J. Struct. Biol.* **2013**, *183*, 278.
[13] L. Addadi, S. Raz, S. Weiner, *Adv. Mater.* **2003**, *15*, 959.
[14] F. Nudelman, K. Pieterse, A. George, P. H. Bomans, H. Friedrich, L. J. Brylka, P. A. Hilbers, G. de With, N. A. Sommerdijk, *Nat. Mater.* **2010**, *12*, 1004.
[15] B. FegleyJr., P. White, H. K. Brown, *Am. Ceram. Soc. Bull.* **1985**, *64*, 1115.
[16] B. Djuričić, D. McGarry, S. Picketing, *J. Mater. Sci. Lett.* **1993**, *12*, 1320.
[17] G. I. Spijksma, H. J. M. Bouwmeester, D. H. A. Blank, V. G. Kessler, *Chem. Commun.* **2004**, *40*, 1874.
[18] a) J. Livage, F. Babonneau, M. Chatry, L. Coury, *Ceram. Int.* **1997**, *23*, 13; b) R. J. Vacassy, C. Guizard, J. Palmeri, L. Cot, *Nanostruct. Mater.* **1998**, *10*, 77; c) C. Viazzi, A. Deboni, J. Z. Ferreira, J-P. Bonino, F. Ansart, *Solid State Sci.* **2006**, *8*, 1023.
[19] C. R. Xia, H. Q. Cao, H. Wang, P. H. Yang, G. Y. Meng, D. K. Peng, *J. Membr. Sci.* **1999**, *162*, 181.
[20] F. Zhang, P. J. Chupas, S. L. A. Lui, J. C. Hanson, W. A. Caliebe, P. L. Lee, S-W. Chan, *Chem. Mater.* **2007**, *19*, 3118.
[21] H. G. Scott, *J. Mater. Sci.* **1975**, *10*, 1527.
[22] C. Wang, M. Zinkevich, F. Aldinger, *CALPHAD* **2004**, *28*, 281.
[23] Z. Ji, J. A. Haynes, E. Voelkl, J. M. Rigsbee, *J. Am. Ceram. Soc.* **2001**, *84*, 929.
[24] E. M. Pouget, P. H. Bomans, J. A. Goos, P. M. Frederik, G. de With, N. A. Sommerdijk, *Science* **2009**, *323*, 1455.
[25] A. Dey, P. H. Bomans, F. A. Müller, J. Will, P. M. Frederik, G. de With, N. A. Sommerdijk, *Nat. Mater.* **2010**, *9*, 1010.
[26] W. J. Habraken, J. Tao, L. J. Brylka, H. Friedrich, L. Bertinetti, A. S. Schenk, A. Verch, V. Dmitrovic, P. H. Bomans, P. M. Frederik, J. Laven, P. van der Schoot, B. Aichmayer, G. de With, J. J. DeYorei, N. A. Sommerdijk, *Nat. Commun.* **2013**, *4*, 1507.
[27] J. Baumgarter, A. Dey, P. H. Boman, C. Le Coadou, P. Fratzl, N. A. Sommerdijk, D. Faivre, *Nat. Mater.* **2013**, *12*, 310.
[28] M. Salavati-Niasari, M. Dadkhah, F. Davar, *Inorg. Chim. Acta.* **2009**, *362*, 3969.
[29] C. Huang, Z. Tang, Z. Zhang, *J. Am. Ceram. Soc.* **2001**, *84*, 1637.
[30] Y. J. Jiang, D. Yang, L. Zhang, Y. Jiang, Y. F. Zhang, J. Li, Z. Y. Jiang, *Ind. Eng. Chem. Res.* **2008**, *47*, 1876.
[31] a) Y. Gao, Y. Masuda, H. Ota, K. Koumoto, *Chem. Mater.* **2004**, *16*, 2615; b) J. Wang, T. J. Shi, X. C. Jiang, *Nanoscale Res. Lett.* **2009**, *4*, 240.
[32] M. J. Collins, C. M. Nielsen-Marsh, J. Hiller, C. T. Smith, J. P. Riberts, R. V. Prigodich, T. J. Wess, J. Csapo, A. R. Millard, G. Turner-Walker, *Archeometry* **2002**, *44*, 383.
[33] X. Guo, T. Schober, *J. Am. Ceram. Soc.* **2004**, *87*, 746.
[34] http://youtu.be/f5fpdUWpUo0 (accessed: November 2013).
[35] J. Mähler, I. Persson, *Inorg. Chem.* **2012**, *51*, 425.
[36] M. Fang, C. H. Kim, G. B. Saupe, H-N. Kim, C. C. Warsksa, T. Miwa, A. Fujishima, T. E. Mallouk, *Chem. Mater.* **1999**, *11*, 1526.
[37] I. L. Cameron, N. J. Short, G. D. Fullerton, *Cell Biol. Int.* **2007**, *31*, 531.
[38] J. P. Orgel, T. C. Irving, A. Miller, T. J. Wess, *Proc. Natl. Acad. Sci. U. S. A.* **2006**, *103*, 9001.
[39] a) W. Tong, C. Gao, H. Möhwald, *Macromol. Rapid. Commun.* **2006**, *27*, 2078; b) C. J. Detzel, A. L. Larkin, P. Rajagopalan, *Tissue Eng. B* **2011**, *17*, 101.